Journal of Hazardous Materials 401 (2021) 123384

Contents lists available at ScienceDirect

Journal of Hazardous Materials

journal homepage: www.elsevier.com/locate/jhazmat

Mercury isotope signatures of a pre-calciner cement plant in Southwest China

Xinyu Li[a,b], Ji Chen[a,c], Li Tang[a,d], Tingting Wu[a,e], Chengcheng Fu[f], Zhonggen Li[a,g,*], Guangyi Sun[a,b], Huifang Zhao[a,b], Leiming Zhang[h], Qiuhua Li[c], Xinbin Feng[a,*]

[a] State Key Laboratory of Environmental Geochemistry, Institute of Geochemistry, Chinese Academy of Sciences, Guiyang, 550081, China
[b] University of Chinese Academy of Sciences, Beijing, 100049, China
[c] Guizhou Provincial Laboratory for Mountainous Environment, Guizhou Normal University, Guiyang, 550001, China
[d] College of Resource and Environmental Engineering, Guizhou University, Guiyang, 550025, China
[e] Key Laboratory of Karst Environment and Geohazard Prevention, Guizhou University, Guiyang, 550003, China
[f] Guizhou Environmental Monitoring Center, Guiyang, 550081, China
[g] College of Resources and Environment, Zunyi Normal University, Zunyi, 563006, China
[h] Air Quality Research Division, Science and Technology Branch, Environment and Climate Change Canada, Toronto, M3H5T4, Canada

GRAPHICAL ABSTRACT

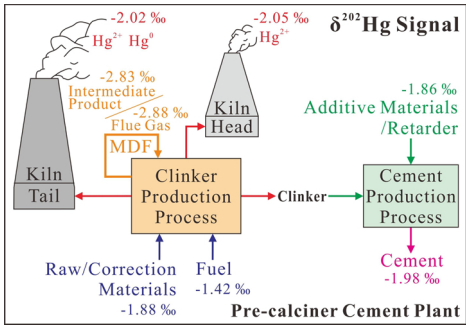

ARTICLE INFO

Editor: J He

Keywords:
Anthropogenic sources
Atmospheric emission
Mass dependent fractionation
Raw meal

ABSTRACT

Characterizing the composition of mercury (Hg) isotopes in the atmospheric emissions of cement plants is critical to understand the global circulation of Hg because large quantities of Hg are released from this source annually. A pre-calciner cement plant in Guizhou Province in Southwest China was selected to investigate the mass dependent fractionation (MDF) and mass independent fractionation (MIF) of Hg in the entire production process and the speciated Hg isotope composition in stack gas. Significant MDF and insignificant MIF were observed in this cement plant. Different raw/correction materials have δ^{202}Hg signals ranging from -1.68 to -2.19‰. Raw meal is featured with lighter Hg (δ^{202}Hg = -2.83 ± 0.18‰) as results of Hg circulation and accumulation during the clinker production. Cement products possess negative δ^{202}Hg values (-1.98 ± 0.02‰) due to the input of light δ^{202}Hg isotopes through additives/retarder limestone, and fly ash and gypsum from coal-fired power plant (CFPPs). Speciated Hg isotopes in the stack gas of the kiln tail and kiln head show no significant differences, and

Abbreviations: Hg, mercury; MDF, mass dependent fractionation; MIF, mass independent fractionation; CFPPs, coal-fired power plants

* Corresponding authors at: State Key Laboratory of Environmental Geochemistry, Institute of Geochemistry, Chinese Academy of Sciences, Guiyang, 550081, China.
E-mail addresses: lizhonggen@mail.gyig.ac.cn (Z. Li), Fengxinbin@mail.gyig.ac.cn (X. Feng).

https://doi.org/10.1016/j.jhazmat.2020.123384
Received 22 October 2019; Received in revised form 29 June 2020; Accepted 2 July 2020
Available online 04 July 2020
0304-3894/

δ^{202}Hg and Δ^{199}Hg in the discharged flue gas averaged at -2.03 ± 0. 31‰ and -0.03 ± 0.07‰, respectively, which has negative δ^{202}Hg characteristics with other anthropogenic sources.

1. Introduction

Mercury (Hg), one of the most toxic heavy metals, has attracted worldwide attention because of its long-range transport in the atmosphere and bioaccumulation in the food chain. Since the devastating Minamata disaster (mercury poisoning disaster) of 1953 in Japan, Hg has been listed as a priority pollutant by many international organizations (UNEP, 2013; WHO, 1991). Hg in the atmosphere is originated from natural (erosion, volcanic eruption) (Lee et al., 2014; Nriagu, 1989; Nriagu and Pacyna, 1988; Pirrone et al., 2010) and anthropogenic sources (fossil fuel combustion, nonferrous metal smelting, cement production, waste incineration) (Lee et al., 2014; Nriagu and Pacyna, 1988; Pirrone et al., 2010; Yu et al., 2015), as well as from the re-emission of previously deposited Hg (e.g., from soil and ocean) (Driscoll et al., 2013; Wang et al., 2018). Substantially increased atmospheric Hg emissions from anthropogenic sources as the industrial revolution have caused adverse effects on the ecological environment (Sarkar et al., 2015; Streets et al., 2017; Wright et al., 2018). Hg emissions from Asia (875–1726 Mg Hg in 2015) accounted for approximately half of the world's total anthropogenic emissions, and China is the largest emitter worldwide with 500–800 Mg Hg emitted to the atmosphere annually (UNEP, 2019).

Major sources of atmospheric Hg in China include fossil fuel combustion, nonferrous metal smelting, and cement production (UNEP, 2019; Wu et al., 2016). Emissions from cement production have increased significantly in recent years (UNEP, 2013, 2019), enabling this sector to be the largest emitter in China since 2009, e.g., approximately 145 Mg Hg was emitted from this source in 2014 (Hua et al., 2016; Wu et al., 2016). Total and speciated atmospheric Hg emissions from this sector have been reported in a few studies (Hua et al., 2016; Li et al., 2019; Won and Lee, 2012), and isotope signatures of Hg emissions from this source have been evaluated by using some proxies such as limestone as raw material, fly ash as an additive, and gypsum as a retarder generated by coal-fired power plants (CFPPs) (Fu et al., 2018; Huang et al., 2016, 2020). However, little is known about the Hg isotope compositions during the entire cement production process and atmospheric emissions based on the on-site studies.

With the progress in cement manufacturing techniques, the use of the pre-calciner process has increased sharply in China since 2000, and over 90 % of cement production has been based on this technique after 2010 (Hua et al., 2016). During the complicated clinker production process, Hg undergoes a series of transformations: it homogenizes in the grinding and homogenizing devices and the raw mill; evaporates in the rotary kiln, pre-calciner, and preheaters; condensates inside the preheater to humidifier; transforms between the rotary kiln and raw mill when the temperature drops; interacts with particulate matter and gaseous components in the flue gas (Mlakar et al., 2010; Wang, 2017; Yang, 2014). Some of these processes may cause Hg isotope fractionation. Therefore, there is a need to investigate the Hg isotope signatures of the upgraded cement plants to better constrain the Hg emission estimates and track Hg emissions from this sector.

In the past twenty years, Hg isotope techniques have been proved powerful for tracking emissions and investigating the global geochemical cycling of Hg (Blum et al., 2014; Feng et al., 2015; Sonke, 2011). In this approach, seven stable Hg isotopes in the nature (Hg^{196}, Hg^{198}, Hg^{199}, Hg^{200}, Hg^{201}, Hg^{202}, and Hg^{204}) and the characteristics of mass-dependent fractionation (MDF) and mass-independent fractionation (MIF) of these isotopes are quantified. In the present study, we

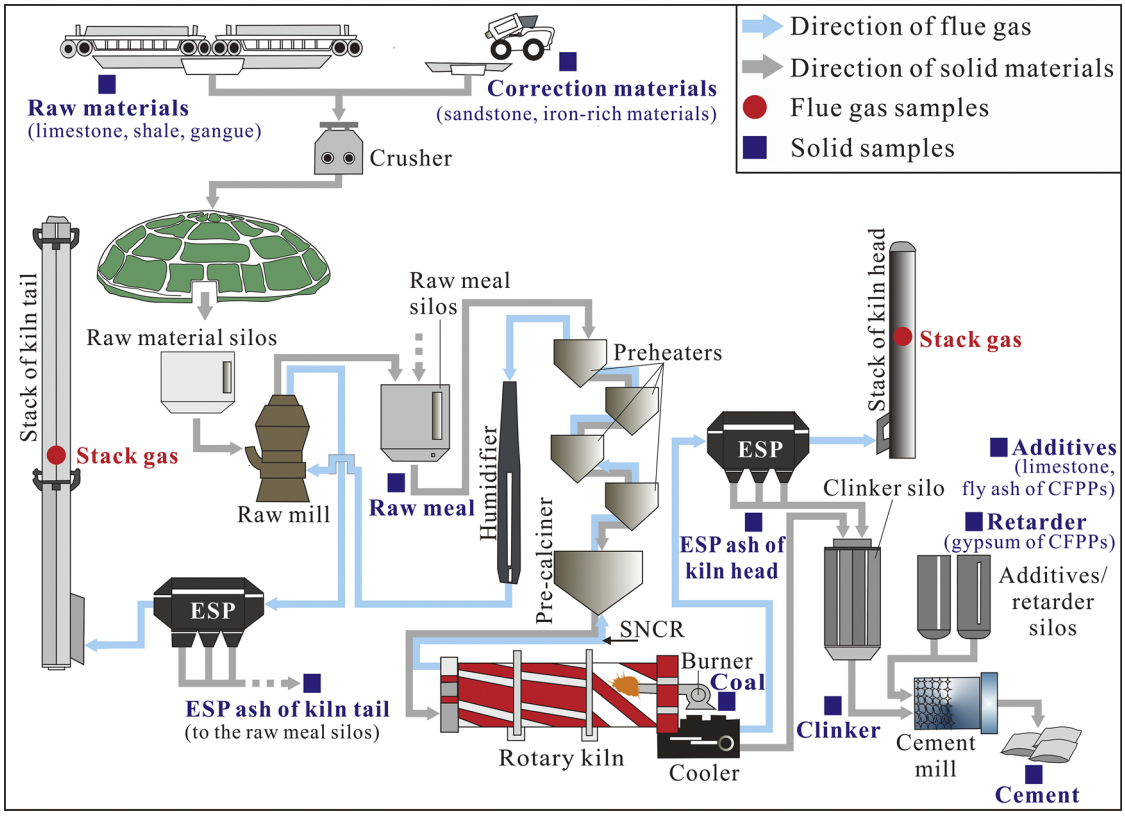

Fig. 1. Schematic diagram of the preheater/pre-calciner cement manufacturing facility and the sampling sites.

systematically collected the solid and gas samples, as well as the material flow information in a cement plant with the pre-calciner process in Guizhou Province, Southwest China, and analyzed the Hg isotope compositions of each type of samples. The objectives of this study are (1) to explore the potential Hg isotope fractionation during the cement production and associated mechanisms and fractionation intensities, and (2) to determine the Hg isotope fingerprints of atmospheric emissions from this source sector. The findings of this study will be helpful to trace the anthropogenic Hg emissions and better understand the Hg geochemistry.

2. Methodology

2.1. Description of the cement plant and the sample collection

The cement plant selected for the investigation is located in east Guizhou Province, Southwest China which is described in a previous study (Li et al., 2019). It has two pre-calciner production lines, each with a capacity of 4500 metric tons of clinker per day. One of the production lines that has been in operation for 1.5 years was investigated in this study. Air pollution control devices (APCDs) of this cement production line include an electrostatic precipitator (ESP) at the kiln head and a selective non-catalytic reduction (SNCR) + ESP at the kiln tail, in which the SNCR is used to control the NOx emissions by spraying urea at the high temperature (800–900 ˚C) zone. All raw and correction materials, such as limestone, sandstone, and shale, were produced locally, with the exception of feed coal, which was transported from Henan and Shaanxi provinces in central China.

The production process and the sampling sites are illustrated in Fig. 1. Solid samples during the clinker and cement production process, as well as stack flue gas samples from the kiln tail and kiln head were collected. Solid samples including various raw (limestone, shale, coal gangue) and correction materials (sandstone, iron-rich materials), fuel (coal), ESP ash from the kiln tail and kiln head, clinker, additive materials (fly ash and gypsum form local CFPPs), and cement products were collected more than three times in three days. Flue gas from the kiln head and kiln tail was sampled using the Ontario Hydro Method (OHM, Model XC-572, Apex Instruments, USA) according to the ASTM Method 6784-02 (2008) (Fig. S1), which can separate three operationally defined Hg species, i.e., gaseous elemental mercury (Hg^0), gaseous oxidized mercury (Hg^{2+}), and particulate mercury (Hg^p). The specific details of the OHM are presented in the supporting information (SI). Each flue gas sample lasted for 1.0–1.5 h with a flue gas volume of 0.5–1.3 m^3.

2.2. Determination and calculation of Hg isotope composition

Solid samples were pretreated in a double-stage tube furnace for Hg isotope analysis (SI) (Huang et al., 2015; Sun et al., 2013a). Hg concentrations in the trapping solutions for solid samples and OHM absorption fluids for flue gas samples were diluted to 1 ng/mL in 10 % acid before Hg isotope analysis. Hg isotope compositions were measured by Nu Plasma II multiple-collector inductively coupled plasma mass spectrometry (MC-ICP-MS, Nu Instruments, UK) equipped with a gas/liquid phase separator (Yin et al., 2010), using $SnCl_2$ (3%, *m/v*) as the reducing agent for Hg to generate gaseous Hg^0, which enters the plasma exciter. Instrumental mass bias correction was accomplished using NIST SRM 997 as an internal standard and external standard-sample bracketing with a NIST SRM 3133 Hg solution. NIST 3133 Hg standard solutions were prepared, with Hg concentrations and acid matrices matched to the sample solutions. MDF and MIF are described in detail in Blum and Bergquist (Blum and Bergquist, 2007) and briefly presented in the SI.

With two chimneys at the kiln tail and kiln head for the cement production line, the final Hg isotope signature of atmospheric emissions was calculated using the equations in the SI. To assess the reliability of Hg isotope composition data, the theoretical Hg isotope compositions of the clinker and the cement production processes were calculated and compared with the results of the MC-ICP-MS (SI).

2.3. Quality assurance and quality control

All vessels used in the isotope analysis were soaked in 20 % HNO_3 and washed with deionized water. Reagents were prepared with deionized water, and HNO_3 and HCl used for Hg pre-concentration in solid samples were double distilled to remove impurities. Hg concentrations of the systematic and reagent blanks were below the detection limit of the MC-ICP-MS. Concerning the reproducibility of the Hg isotope data, certified reference materials (CRMs, UM-Almadén and NIST SRM 1632d (coal)) were analyzed along with the diluted acid-trapping and OHM solutions. The recovery of total Hg in solid samples and CRM (coal) during the pre-concentration process by double-stage furnace trapping was in the range of 87–98 %. The Hg isotope compositions of CRMs in this study are in good agreement with the previously published data (Table 1) (Blum and Bergquist, 2007; Estrade et al., 2010; Sun et al., 2013a, 2014).

3. Results and discussion

3.1. Hg isotope compositions along the cement plant production

The Hg concentrations in various solid/gas materials, main Hg inputs and outputs from different processes, and atmospheric Hg emissions from the cement plant are reported in our previous study (Li et al., 2019) and also presented in Table S1 and Table S2. Raw and correction materials, as the main Hg input for the tested cement plant, accounted for 84.8 % of total Hg input; limestone contributed to 56.5 % and coal contributed to 15.2 % of total Hg input. Hg emissions are in the form of Hg^{2+} (54.8 %) and Hg^0 (45.1 %) at the stack of the kiln tail, whereas they are primarily in the form of Hg^{2+} (98.1 %) at the kiln head. Considering the low proportion of Hg^p in total Hg (< 0.1 %, Table S2) and the difficulty in detecting the isotope composition of Hg^0 and Hg^p at low concentrations (0.01–0.29 μg/m^3) in the flue gas, only Hg^{2+} (7.93 μg/m^3) and Hg^0 (6.52 μg/m^3) in the stack flue gas of the kiln tail and Hg^{2+} (16.33 μg/m^3) in the stack flue gas of the kiln head were analyzed in this study. Clinker was not subject to the isotope analysis because of its low Hg concentration (< 1 μg/kg) and low contribution to the Hg mass flow (Table S1). Hg isotope compositions in stack gas, raw and correction materials, and final cement products are presented in Table 2, Table S3, and Fig. 2.

Table 1
Hg isotope compositions (‰) in certified reference materials (CRMs) reported in this study and others.

CRMs	$\delta^{199}Hg$	2σ	$\delta^{200}Hg$	2σ	$\delta^{201}Hg$	2σ	$\delta^{202}Hg$	2σ	$\Delta^{199}Hg$	2σ	$\Delta^{200}Hg$	2σ	$\Delta^{201}Hg$	2σ	Reference
UM-Almadén (N = 12)	−0.14	0.06	−0.26	0.05	−0.43	0.08	−0.51	0.06	−0.02	0.05	0.00	0.03	−0.04	0.05	This study
UM-Almadén (N = 25)	−0.14	0.06	−0.27	0.04	−0.44	0.07	−0.54	0.08	−0.01	0.02	0.00	0.02	−0.04	0.04	(Blum and Bergquist, 2007)
UM-Almadén (N = 10)	−0.14	0.09	−0.26	0.10	−0.41	0.11	−0.51	0.15	−0.01	0.07	−0.01	0.06	−0.03	0.04	(Estrade et al., 2010)
NIST 1632d (N = 7)	−0.53	0.11	−0.99	0.13	−1.50	0.21	−1.93	0.19	−0.04	0.07	−0.02	0.05	−0.05	0.08	This study
NIST 1632d (N = 8)	−0.50	0.03	−0.91	0.09	−1.39	0.18	−1.83	0.14	−0.04	0.05	0.01	0.06	−0.02	0.09	(Sun et al., 2013a)
NIST 1632d (N = 10)	−0.49	0.06	−0.89	0.09	−1.37	0.18	−1.79	0.17	−0.04	0.05	−0.01	0.06	−0.03	0.08	(Sun et al., 2014)

Table 2
Average Hg isotope compositions in solid materials and stack flue gas of the cement plant determined by MC-ICP-MS.

Productive process	Item	Samples (N represents the sample number)	Hg isotope composition (‰)													
			δ^{199}Hg	σ	δ^{200}Hg	σ	δ^{201}Hg	σ	δ^{202}Hg	σ	Δ^{199}Hg	σ	Δ^{200}Hg	σ	Δ^{201}Hg	σ
Clinker process	Raw materials	Limestone (N = 3)	−0.41	0.12	−0.84	0.13	−1.31	0.15	−1.68	0.20	0.01	0.08	0.00	0.04	−0.04	0.04
		Shale (N = 2)	−0.61	0.05	−0.89	0.02	−1.50	0.00	−1.78	0.10	−0.16	0.07	0.00	0.07	−0.17	0.08
		Gangue (N = 2)	−0.39	0.34	−0.98	0.79	−1.46	1.16	−2.06	1.54	0.12	0.04	0.05	0.02	0.08	0.00
	Correction materials	Sandstone (N = 3)	−0.77	0.02	−1.09	0.07	−1.91	0.14	−2.19	0.11	−0.22	0.02	0.01	0.04	−0.26	0.05
		Iron-rich materials (N = 3)	−0.40	0.03	−0.79	0.06	−1.20	0.11	−1.68	0.07	0.02	0.01	0.06	0.04	0.06	0.06
	Fuel	Coal (N = 2)	−0.34	0.04	−0.68	0.35	−1.07	0.48	−1.42	0.82	0.02	0.17	0.04	0.06	0.00	0.13
	Stack gas of kiln tail	Hg^{2+} (N = 2)	−0.56	0.11	−0.94	0.31	−1.52	0.52	−1.86	0.71	−0.09	0.07	−0.01	0.04	−0.12	0.02
		Hg^0 (N = 2)	−0.52	0.03	−1.06	0.17	−1.66	0.19	−2.22	0.29	0.04	0.10	0.06	0.03	0.01	0.03
	Stack gas of kiln head	Hg^{2+} (N = 3)	−0.53	0.05	−0.99	0.02	−1.60	0.03	−2.05	0.01	−0.02	0.05	0.04	0.02	−0.06	0.02
	Intermediate products	Raw meal (N = 3)	−0.79	0.05	−1.36	0.10	−2.14	0.19	−2.83	0.18	−0.08	0.05	0.06	0.02	−0.01	0.08
		ESP ash of kiln tail (N = 4)	−0.71	0.06	−1.17	0.12	−1.88	0.16	−2.40	0.24	−0.10	0.01	0.03	0.01	−0.08	0.04
Cement production process	Additive materials	Fly ash of CFPPs (N = 3)	−0.59	0.14	−1.06	0.22	−1.62	0.29	−2.29	0.42	−0.01	0.03	0.09	0.02	0.10	0.03
		Limestone (N = 3)	−0.41	0.12	−0.84	0.13	−1.31	0.15	−1.68	0.20	0.01	0.08	0.00	0.04	−0.04	0.04
	Retarder	Gypsum of CFPPs (N = 3)	−0.50	0.05	−0.74	0.09	−1.30	0.15	−1.62	0.20	−0.10	0.06	0.07	0.05	−0.08	0.05
	Product	Cement (N = 2)	−0.48	0.07	−1.03	0.02	−1.46	0.02	−1.98	0.02	0.02	0.06	−0.04	0.03	0.03	0.01

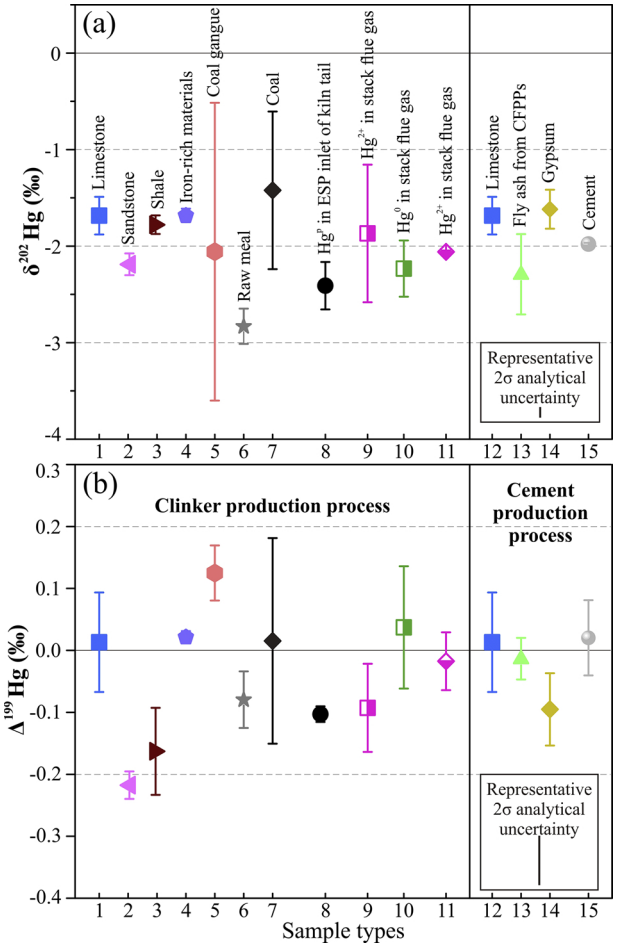

Fig. 2. Hg isotope composition of δ^{202}Hg (a) and Δ^{199}Hg (b) in solid and flue gas samples of the pre-calciner cement plant.

All solid and flue gas samples in the tested cement plant are characterized by significant negative MDF values of Hg (Fig. 2a), with a variation of 1.41‰ in δ^{202}Hg (-2.83‰ to -1.42‰). Negative δ^{202}Hg values were observed in the raw/correction materials and coal, e.g., limestone (-1.68 ± 0.20‰, 1σ, N = 3), sandstone (-2.19 ± 0.11‰, 1σ, N = 3), shale (-1.78 ± 0.10‰, 1σ, N = 2), iron-rich material (-1.68 ± 0.07‰, 1σ, N = 3), gangue (-2.06 ± 1.54‰, 1σ, N = 2), and coal (-1.42 ± 0.82‰, 1σ, N = 2). Raw meal, an intermediate product, is enriched in light Hg isotopes (δ^{202}Hg = -2.83 ± 0.18‰, 1σ, N = 3, $p < 0.01$) compared to the other samples. As for the flue gas, δ^{202}Hg of Hg^{2+} (-1.86 ± 0.71‰, 1σ, N = 2) is somewhat similar to that of Hg^0 (-2.22 ± 0.29‰, 1σ, N = 2) in the stack gas from the kiln tail (the number of samples is too small for statistical comparison), and no significant difference in MDF ($p = 0.10$) was observed between the stack gas from the kiln head (Hg^{2+}, δ^{202}Hg = -2.05 ± 0.01‰, 1σ, N = 4) and kiln tail (-1.86 ± 0.71‰ for Hg^{2+}, -2.22 ± 0.29‰ for Hg^0, and -2.02 ± 0.52‰ for total Hg). δ^{202}Hg in fly ash and gypsum from CFPPs used in cement production process averaged at -2.29 ± 0.42‰ (1σ, N = 3) and -1.62 ± 0.20‰ (1σ, N = 3), respectively. These figures are dependent on the fuel type, combustion process, and the APCDs installed in CFPPs (Sun et al., 2013b; Tang et al., 2017). Finally, δ^{202}Hg in cement products was -1.98 ± 0.02‰ (1σ, N = 3).

Δ^{199}Hg varied by 0.34‰ (-0.22 to 0.12‰) in solid and flue gas samples from the tested cement plant; however, no significant ($p > 0.05$) difference was observed in the mean Δ^{199}Hg values between the input materials, intermediate products, and stack gas/output production in the clinker or cement production process (Fig. 2b). Δ^{199}Hg of raw/correction materials and additive/retarder materials are in the range of -0.22 – 0.12‰ and -0.10 – 0.01‰, respectively. The average Δ^{199}Hg signatures of raw meal (intermediate product) and cement (output production) are -0.08 ± 0.05‰ (N = 3, 1σ) and 0.02 ± 0.06‰ (N = 2, 1σ), respectively. Moreover, there is no significant ($p > 0.05$) difference in Δ^{199}Hg between the stack gas from the kiln tail (-0.14 – 0.11‰) and kiln head (-0.07 – 0.02‰). Δ^{199}Hg values of solid and flue gas samples approximated zero (-0.22 – 0.12‰), considering that the 2σ analytical uncertainty is 0.08‰ for Δ^{199}Hg (N = 42) in this study (Fig. 2b), which indicates the absence of the MIF processes in the cement plant.

3.2. Reliability of Hg isotope data

The reliability of Hg isotope composition data was evaluated separately for the clinker and cement production processes, as detailed in the SI. The production line in the cement plant has a total Hg mass balance ratio of 101 % and 93 % for the output/input in the clinker and the cement production processes, respectively (Table S1) (Li et al., 2019). The reliability of Hg isotope composition data of the output products of the cement plant is shown in Fig. S2. The calculated values of δ^{202}Hg and Δ^{199}Hg are -1.71 ± 0.37‰ (1σ) and 0.01 ± 0.08‰ (1σ)

for stack gas, and -1.65 ± 0.22‰ (1σ) and -0.08 ± 0.06‰ (1σ) for cement production, respectively. These values are not statistically different from those measured by the MC-ICP-MS at the 2σ analytical uncertainty (Table 1, δ^{202}Hg and Δ^{199}Hg of stack gas were calculated using Eq. 5 and Eq. 6 in the SI), indicating that the Hg isotope data in this study are reliable and Hg isotopes in input and output substances reach an equilibrium in the clinker and cement production processes.

3.3. MDF in the clinker production process

Large amounts of sedimentary rocks, such as limestone, sandstone, and shale were used as raw/correction materials in the clinker production process, which were preferentially enriched with light Hg isotopes from the ocean or surface water during the sedimentation process (Blum and Johnson, 2017; Hoefs, 2018). Limestone enriched with light Hg isotopes (δ^{202}Hg = -1.42 to -1.64‰) has been reported in previous studies (Sun et al., 2016; Wang et al., 2015). Similar to certain organic minerals, the negative value of δ^{202}Hg for gangue is related to the preferential absorption and utilization of light Hg isotopes by plants (Blum and Johnson, 2017; Yin et al., 2013a). As one of the critical ingredients for producing high-quality clinker, iron-rich materials are mainly composed of iron ore (Fe_2O_3), which also has a negative δ^{202}Hg (-1.68 ± 0.07‰, 1σ, N = 3) in this study.

The coal used in this cement plant was from Henan and Shaanxi provinces; both are major coal production areas in China. The isotope compositions of Hg show significant differences between the coals from these two provinces, with moderately negative δ^{202}Hg (-2.00‰, N = 1) in Henan and slightly negative δ^{202}Hg (-0.84‰, N = 1) in Shaanxi coal, which might be the result of different coal forming plants and external input materials in the local environment (Biswas et al., 2008; Sun et al., 2016).

Raw meal is featured with the most negative δ^{202}Hg (-2.83 ± 0.18‰) signal in the clinker production process, although it is composed of grinded and homogenized raw/correction materials (-2.32 to -1.47‰) after the raw mill. Huang et al. (2016) reported a δ^{202}Hg value of -1.99‰ for raw meal in a cement plant in Sichuan, China, which is also more negative than δ^{202}Hg values (-1.79 to -1.02‰) of raw/correction materials of limestone, clay, and sandstone. This result reflected the existence of MDF in the clinker production process. Li et al. (2019) reported that the total Hg pool in raw meal is approximately six times the daily input from various raw/correction materials and fuels in the cement plant, indicating the accumulation of Hg in the clinker production process.

The existence of more lighter Hg isotopes in raw meal than raw/correction materials can be explained by Hg accumulation as results of external and internal Hg circulation in the clinker production process. The internal circulation refers to the circulation of Hg between the raw mill and the rotary kiln system. Hg with light isotopes preferentially enters the gas phase during volatilization, resulting in lighter Hg in the gas phase and heavier Hg in the residual phase (Zheng et al., 2007). Lighter Hg is vaporized as Hg^0 into the flue gas from high temperature-heated raw meal, and heavier Hg remains in the semi-finished clinker when the rotary kiln and pre-calciner are at high temperatures (800–1450 °C) (Huang et al., 2016). With the high-temperature flue gas returning to the cryogenic equipment (humidification tower and raw mill, 90–330 °C) and cooling down, Hg^0 in flue gas is oxidized into Hg^{2+} by other components in the flue gas, such as chlorine, oxygen, or metal oxides (Yang and Pan, 2007; Zhang et al., 2016; Zhou et al., 2015). Most of Hg^0 and Hg^{2+} in the flue gas are captured by particulate matter and mixed with the raw/correction materials at the raw mill and re-enter the raw meal silos, pre-heaters, pre-calciner, and the rotary kiln system and re-evaporate (Li et al., 2019; Wang et al., 2014). Hg species would not change inside the SNCR because they are thermodynamically stable species of Hg^0 at temperatures higher than 800 °C (Zhang et al., 2016). Based on the Hg isotope mass balance for the kiln tail and kiln head system (Fig. S3), the calculated δ^{202}Hg values in the returned flue gas of the raw mill are -2.91 ± 0.17‰ and -2.86 ± 0.21‰ for the kiln tail and kiln head, respectively (Table S4, calculations are presented in SI), suggesting that significant MDF occurred in the pre-calciner, preheater, and exiting flue gas, which would explain the much lighter Hg isotopes in raw meal than different raw/correction materials.

The external one refers to the reuse of ESP ash from the kiln tail as a clinker production material that is sent back to the raw meal silo. ESP ash from the kiln tail is enriched with lighter isotopes of Hg (δ^{202}Hg of -2.40 ± 0.2‰) than gaseous Hg^{2+} (δ^{202}Hg = -1.86 ± 0.71‰) and Hg^0 (δ^{202}Hg = -2.22 ± 0.29‰) in the stack gas of the kiln tail, indicating that ESP ash accumulated lighter Hg isotopes during the dust removal process. Thus, Hg accumulation in the external (recycling of ESP ash) and internal Hg circulation (returning of flue gas into raw mill) in the clinker production process brought a large amount of lighter Hg isotopes into the raw mill and raw meal silo, featuring raw meal with more lighter Hg isotopes than raw/correction materials.

3.4. Mixture effect of Hg isotopes in the cement production process

The cement production process refers to the blending of the clinker with the additive material, such as limestone, coal combustion ash, and retarders such as gypsum. Coal combustion products show significant differences in Hg MDF signals (Sun et al., 2013b; Tang et al., 2017). Fly ash has more negative δ^{202}Hg (-2.29 ± 0.42‰) than gypsum (-1.62 ± 0.20‰) obtained from the same local CFPP in this study owing to the successive production or removal by particulate matter collectors and flue gas desulfurization devices, respectively (Huang et al., 2017; Liu et al., 2019). Limestone has a δ^{202}Hg value of -1.68 ± 0.20‰ and is also used as an additive in addition to its use as raw material. After various materials were homogenized in the cement mill, δ^{202}Hg of the cement products (-1.98 ± 0.02‰) was in the middle of those of additive and retarder materials (-1.62 to -2.29‰) because nearly all Hg in cement is derived from these materials (Li et al., 2019).

3.5. Hg isotope signatures of atmospheric emissions

According to the proportion of speciated Hg (54.8 % Hg^{2+} and 45.1 % Hg^0) in the stack gas of the kiln tail, the weighted δ^{202}Hg and Δ^{199}Hg values of total Hg were calculated as -2.02 ± 0.52‰ and -0.03 ± 0.08‰, respectively (Table 2). Moreover, the values of δ^{202}Hg and Δ^{199}Hg in the stack gas of the kiln head were -2.05 ± 0.01‰ and -0.02 ± 0.05‰, respectively, which was related to the Hg isotope composition of both feed coals and flue gas escaping the rotary kiln. Hg isotope signatures of atmospheric emissions from this cement plant have integrated δ^{202}Hg and Δ^{199}Hg of -2.03 ± 0.31‰ and -0.03 ± 0.07‰, respectively, based on Eq. 5 and Eq. 6 in the SI, incorporating the emissions from both the kiln tail and kiln head.

Hg isotope compositions of important anthropogenic Hg sources, including coal, gold ore, Hg ore, sphalerites, and stack emissions from CFPPs, are illustrated in Fig. 3 (Cooke et al., 2013; Feng et al., 2013; Huang et al., 2017; Liu et al., 2019; Smith, 2010; Stetson et al., 2009; Sun et al., 2016; Tang et al., 2017; Wiederhold et al., 2013; Yin et al., 2016, 2013b). The Hg isotope signature of atmospheric emissions from the cement plant is significantly more negative ($p < 0.01$) than those of other anthropogenic sources of δ^{202}Hg. As for MIF, on-site stack emissions from CFPPs (-3.21 to 0.25‰) have more negative Δ^{199}Hg signals (Tang et al., 2017); however, there is insignificant signal for Δ^{199}Hg from this cement plant, which is identical to world coal, gold ore, Hg ore, and sphalerites (Cooke et al., 2013; Feng et al., 2013; Huang et al., 2017; Smith, 2010; Stetson et al., 2009; Sun et al., 2016; Wiederhold et al., 2013; Yin et al., 2016, 2013b). Therefore, atmospheric emissions of cement plants have a critical impact on the negative δ^{202}Hg of atmospheric Hg, and this unique negative δ^{202}Hg signal and near-zero Δ^{199}Hg can be used to distinguish this source from other anthropogenic Hg sources in source apportionment analysis.

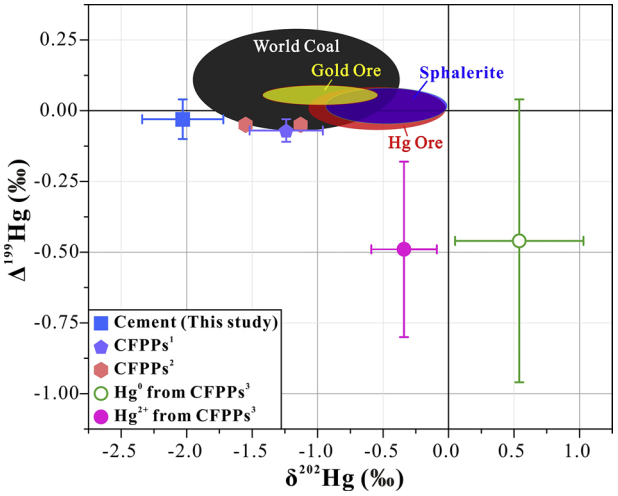

Fig. 3. Comparison of Hg isotope composition in atmospheric emissions from the cement plant and other anthropogenic sources.
world coal: (Sun et al., 2016); gold ore: (Smith, 2010); sphalerite: (Yin et al., 2016); Hg ore: (Cooke et al., 2013; Feng et al., 2013; Stetson et al., 2009; Wiederhold et al., 2013; Yin et al., 2013b). 1, 2: Calculated stack emissions from CFPPs in North (Liu et al., 2019) and Southeast China (Huang et al., 2017), respectively; 3: On-site Hg° and Hg^{2+} in stack emissions from CFPPs in North China (Tang et al., 2017).

4. Conclusions

Mercury isotope signatures in a large-scale pre-calciner cement plant in Southwest China were characterized based on the analysis of Hg isotopes in solid and flue gas samples. There are significant MDF and insignificant MIF in the cement plant. All samples have a negative value of Hg isotope composition, with 1.41‰ variation in δ^{202}Hg (-2.83 to -1.42‰) in clinker production as a result of internal and external cycling of Hg. Hg isotope composition in the returned flue gas of the raw mill is lighter than that of raw/correction materials. Similarly, recycling ESP ash from the kiln tail may also lighten the δ^{202}Hg signals in raw meal because of the dust removed by ESP featured with negative δ^{202}Hg signals. Mass-weighted δ^{202}Hg and Δ^{199}Hg of atmospheric Hg emissions from this pre-calciner cement plant have values of -2.03 ± 0. 31‰ and -0.03 ± 0.07‰, respectively. δ^{202}Hg in the output cement products mostly depends on those of additive and retarder materials and has a value of -1.98 ± 0.02‰.

There are some differences in Hg isotope compositions between the tested cement plant and previously reported CFPPs and other anthropogenic sources. Although significant MDF occurred in the clinker production process, the discharged Hg into atmosphere is featured with δ^{202}Hg and Δ^{199}Hg signals that are close to those of raw/correction materials. This result is different from the case of CFPPs with high Hg removal efficiencies with different APCDs (Liu et al., 2019; Sun et al., 2013b; Tang et al., 2017). However, further on-site studies should be conducted in different pre-calciner cement plants in various locations and with different raw/correction materials to reduce the uncertainties in Hg isotope signals of this source. In addition, more Hg isotope analysis should be conducted for intermediate products (raw meal, clinker, ESP ash, and intermediate flue gas) to obtain a more vivid picture of δ^{202}Hg fractionation inside the pre-calciner cement plants.

CRediT authorship contribution statement

Xinyu Li: Formal analysis, Methodology, Software, Visualization, Writing - original draft, Writing - review & editing. **Ji Chen:** Investigation. **Li Tang:** Investigation. **Tingting Wu:** Investigation. **Chengcheng Fu:** Funding acquisition, Investigation, Project administration. **Zhonggen Li:** Conceptualization, Data curation, Formal analysis, Funding acquisition, Investigation, Project administration, Resources, Supervision, Validation, Writing - review & editing. **Guangyi Sun:** Methodology. **Huifang Zhao:** Methodology. **Leiming Zhang:** Writing - review & editing. **Qiuhua Li:** Methodology. **Xinbin Feng:** Conceptualization, Funding acquisition, Project administration, Resources, Supervision.

Declaration of Competing Interest

The authors declare that they have no known competing financial interests or personal relationships that could have appeared to influence the work reported in this paper.

Acknowledgements

This work is financially supported by the Environmental Science and Technology Project of Guizhou Environmental Protection Department (No. [2013] 8), Opening Fund of the State Key Laboratory of Environmental Geochemistry (SKLEG2020206), the Natural Science Foundation of China (No. U1612442), the Doctoral Foundation Project of Zunyi Normal University (No. Zun-Shi BS [2018]15), and K. C. Wong Education Foundation.

Appendix A. Supplementary data

Supplementary material related to this article can be found, in the online version, at doi:https://doi.org/10.1016/j.jhazmat.2020.123384.

References

Biswas, A., Blum, J.D., Bergquist, B.A., Keeler, G.J., Xie, Z., 2008. Natural mercury isotope variation in coal deposits and organic soils. Environ. Sci. Technol. 42, 8303–8309.
Blum, J.D., Bergquist, B.A., 2007. Reporting of variations in the natural isotopic composition of mercury. Anal. Bioanal. Chem. 388, 353–359.
Blum, J.D., Johnson, M.W., 2017. Recent developments in mercury stable isotope analysis. Rev. Mineral. Geochem. 82, 733–757.
Blum, J.D., Sherman, L.S., Johnson, M.W., 2014. Mercury isotopes in earth and environmental sciences. Annu. Rev. Earth Planet. Sci. 42, 249–269.
Cooke, C.A., Hintelmann, H., Ague, J.J., Burger, R., Biester, H., Sachs, J.P., Engstrom, D.R., 2013. Use and legacy of mercury in the Andes. Environ. Sci. Technol. 47, 4181–4188.
Driscoll, C.T., Mason, R.P., Hing Man, C., Jacob, D.J., Nicola, P., 2013. Mercury as a global pollutant: sources, pathways, and effects. Environ. Sci. Technol. 47, 4967–4983.
Estrade, N., Carignan, J., Sonke, J.E., Donard, O.F.X., 2010. Measuring Hg isotopes in bio-geo-environmental reference materials. Geostand. Geoanal. Res. 34, 79–93.
Feng, X., Yin, R., Yu, B., Du, B., 2013. Mercury isotope variations in surface soils in different contaminated areas in Guizhou Province, China. Chin. Sci. Bull. 58, 249–255.
Feng, X., Yin, R., Yu, B., Du, B., Chen, J., 2015. A review of Hg isotope geochenistry. Earth Sci. Front. 22, 124–135 (In Chinese with English abstract).
Fu, X., Yang, X., Tan, Q., Ming, L., Lin, T., Lin, C.-J., Li, X., Feng, X., 2018. Isotopic composition of gaseous elemental mercury in the marine boundary layer of East China Sea. J. Geophys. Res. Atmos. 123, 7656–7669.
Hoefs, J., 2018. Stable Isotope Geochemistry, eighth edition. .
Hua, S., Tian, H., Wang, K., Zhu, C., Gao, J., Ma, Y., Xue, Y., Wang, Y., Duan, S., Zhou, J., 2016. Atmospheric emission inventory of hazardous air pollutants from China's cement plants: temporal trends, spatial variation characteristics and scenario projections. Atmos. Environ. 128, 1–9.
Huang, Q., Liu, Y., Chen, J., Feng, X., Huang, W., Yuan, S., Cai, H., Fu, X., 2015. An improved dual-stage protocol to pre-concentrate mercury from airborne particles for precise isotopic measurement. J. Anal. At. Spectrom. 30, 957–966.
Huang, Q., Chen, J., Huang, W., Fu, P., Guinot, B., Feng, X., Shang, L., Wang, Z., Wang, Z., Yuan, S., Cai, H., Wei, L., Yu, B., 2016. Isotopic composition for source identification of mercury in atmospheric fine particles. Atmos. Chem. Phys. 16, 11773–11786.
Huang, S., Yuan, D., Lin, H., Sun, L., Lin, S., 2017. Fractionation of mercury stable isotopes during coal combustion and seawater flue gas desulfurization. Appl. Geochem. 76, 159–167.
Huang, Q., Reinfelder, J.R., Fu, P., Huang, W., 2020. Variation in the mercury concentration and stable isotope composition of atmospheric total suspended particles in Beijing, China. J. Hazard. Mater. 383, 121131.
Lee, G., Kim, P., Han, Y., Holsen, T., Lee, S., 2014. Tracing sources of total gaseous mercury to Yongheung Island off the coast of Korea. Atmos 5, 273–291.
Li, X., Li, Z., Wu, T., Chen, J., Fu, C., Zhang, L., Feng, X., Fu, X., Tang, L., Wang, Z., Wang, Z., 2019. Atmospheric mercury emissions from two pre-calciner cement plants in

Southwest China. Atmos. Environ. 199, 177–188.
Liu, H., Diao, X., Yu, B., Shi, J., Liu, Q., Yin, Y., Hu, L., Yuan, C., Jiang, G., 2019. Effect of air pollution control devices on mercury isotopic fractionation in coal-fired power plants. Chem. Geol. 517, 1–6.
Mlakar, T.L., Horvat, M., Vuk, T., Stergaršek, A., Kotnik, J., Tratnik, J., Fajon, V., 2010. Mercury species, mass flows and processes in a cement plant. Fuel 89, 1936–1945.
Nriagu, J.O., 1989. A global assessment of natural sources of atmospheric trace metals. Nature 338, 47–49.
Nriagu, J.O., Pacyna, J.M., 1988. Quantitative assessment of worldwide contamination of air, water and soils by trace metals. Nature 333, 134–139.
Pirrone, N., Cinnirella, S., Feng, X., Finkelman, R.B., Friedli, H.R., Leaner, J., Mason, R., Mukherjee, A.B., Stracher, G.B., Streets, D.G., Telmer, K., 2010. Global mercury emissions to the atmosphere from anthropogenic and natural sources. Atmos. Chem. Phys. 10, 5951–5964.
Sarkar, S., Ahmed, T., Swami, K., Judd, C.D., Bari, A., Dutkiewicz, V.A., Husain, L., 2015. History of atmospheric deposition of trace elements in lake sediments, ~1880 to 2007. J. Geophys. Res. Atmos. 120, 5658–5669.
Smith, C., 2010. Isotopic Geochemistry of Mercury in Active and Fossil Hydrothermal Systems. University of Michigan.
Sonke, J.E., 2011. A global model of mass independent mercury stable isotope fractionation. Geochim. Cosmochim. Acta 75, 4577–4590.
Stetson, S.J., Gray, J.E., Wanty, R.B., Macalady, D.L., 2009. Isotopic variability of mercury in ore, mine-waste calcine, and leachates of mine-waste calcine from areas mined for mercury. Environ. Sci. Technol. 43, 7331–7336.
Streets, D.G., Horowitz, H.M., Jacob, D.J., Lu, Z., Levin, L., Ter Schure, A.F.H., Sunderland, E.M., 2017. Total mercury released to the environment by human activities. Environ. Sci. Technol. 51, 5969–5977.
Sun, R., Enrico, M., Heimburger, L.E., Scott, C., Sonke, J.E., 2013a. A double-stage tube furnace-acid-trapping protocol for the pre-concentration of mercury from solid samples for isotopic analysis. Anal. Bioanal. Chem. 405, 6771–6781.
Sun, R., Heimbürger, L.-E., Sonke, J.E., Liu, G., Amouroux, D., Berail, S., 2013b. Mercury stable isotope fractionation in six utility boilers of two large coal-fired power plants. Chem. Geol. 336, 103–111.
Sun, R., Sonke, J.E., Heimbürger, L.-E., Belkin, H.E., Liu, G., Shome, D., Cukrowska, E., Liousse, C., Pokrovsky, O.S., Streets, D.G., 2014. Mercury stable isotope signatures of world coal deposits and historical coal combustion emissions. Environ. Sci. Technol. 48, 7660–7668.
Sun, R., Sonke, J.E., Liu, G., 2016. Biogeochemical controls on mercury stable isotope compositions of world coal deposits: a review. Earth-Sci. Rev. 152, 1–13.
Tang, S., Feng, C., Feng, X., Zhu, J., Sun, R., Fan, H., Wang, L., Li, R., Mao, T., Zhou, T., 2017. Stable isotope composition of mercury forms in flue gases from a typical coal-fired power plant, Inner Mongolia, northern China. J. Hazard. Mater. 328, 90–97.
UNEP, 2013. Global Mercury Assessment 2013: Sources, Emissions, Releases and Environmental Transport. UNEP Chemicals Branch, Geneva, Switzerland.
UNEP, 2019. Global Mercury Assessment 2018. Chemicals and Health Branch, Geneva, Switzerland.
Wang, X.L., 2017. Research on the Characteristics of Mercury Emission and the Potention of Emission Reduction in the Process of Cement Production. Zhejiang University (In Chinese with English abstract).
Wang, F., Wang, S., Zhang, L., Yang, H., Wu, Q., Hao, J., 2014. Mercury enrichment and its effects on atmospheric emissions in cement plants of China. Atmos. Environ. 92, 421–428.
Wang, Z., Chen, J., Feng, X., Hintelmann, H., Yuan, S., Cai, H., Huang, Q., Wang, S., Wang, F., 2015. Mass-dependent and mass-independent fractionation of mercury isotopes in precipitation from Guiyang, SW China. IEEE Trans. Geosci. Remote Sens. 347, 358–367.
Wang, X., Lin, C.-J., Feng, X., Yuan, W., Fu, X., Zhang, H., Wu, Q., Wang, S., 2018. Assessment of regional mercury deposition and emission outflow in mainland China. J. Geophys. Res. Atmos. 123, 9868–9890.
WHO, 1991. Environmental health criteria. Inorganic Mercury, vol. 118 World Health Organization, Geneva.
Wiederhold, J.G., Smith, R.S., Siebner, H., Jew, A.D., Brown Jr, G.E., Bourdon, B., Kretzschmar, R., 2013. Mercury isotope signatures as tracers for Hg cycling at the New Idria Hg Mine. Environ. Sci. Technol. 47, 6137–6145.
Won, J.H., Lee, T.G., 2012. Estimation of total annual mercury emissions from cement manufacturing facilities in Korea. Atmos. Environ. 62, 265–271.
Wright, L.P., Zhang, Leiming, Cheng, I., Aherne, J., Wentworth, G.R., 2018. Impacts and effects indicators of atmospheric deposition of major pollutants to various ecosystems-A review. Aerosol Air Qual. Res. 18, 1953–1992.
Wu, Q., Wang, S., Li, G., Liang, S., Lin, C.J., Wang, Y., Cai, S., Liu, K., Hao, J., 2016. Temporal trend and spatial distribution of speciated atmospheric mercury emissions in China during 1978-2014. Environ. Sci. Technol. 50, 13428–13435.
Yang, H., 2014. Study on Atmospheric Mercury Emission and Control Strategies From Cement Production in China. Tsinghua University (In Chinese with English abstract).
Yang, H., Pan, W., 2007. Transformation of mercury speciation through the SCR system in power plants. J. Environ. Sci. China (China) 19, 181–184.
Yin, R.S., Feng, X.B., Foucher, D., Shi, W.F., Zhao, Z.Q., Wang, J., 2010. High precision determination of mercury isotope ratios using online mercury vapor generation system coupled with multicollector inductively coupled plasma-mass spectrometer. Chinese J. Anal. Chem. 38, 929–934.
Yin, R., Feng, X., Meng, B., 2013a. Stable mercury isotope variation in rice plants (Oryza sativa L.) from the Wanshan mercury mining district, SW China. Environ. Sci. Technol. 47, 2238–2245.
Yin, R., Feng, X., Wang, J., Li, P., Liu, J., Zhang, Y., Chen, J., Zheng, L., Hu, T., 2013b. Mercury speciation and mercury isotope fractionation during ore roasting process and their implication to source identification of downstream sediment in the Wanshan mercury mining area, SW China. Chem. Geol. 336, 72–79.
Yin, R., Feng, X., Hurley, J.P., Krabbenhoft, D.P., Lepak, R.F., Hu, R., Zhang, Q., Li, Z., Bi, X., 2016. Mercury isotopes as proxies to identify sources and environmental impacts of mercury in sphalerites. Sci. Rep. 6, 18686.
Yu, B., Wang, X., Lin, C.J., Fu, X., Zhang, H., Shang, L., Feng, X., 2015. Characteristics and potential sources of atmospheric mercury at a subtropical near-coastal site in East China. J. Geophys. Res. Atmos. 120 (2015), 8563–8574.
Zhang, L., Wang, S.X., Wu, Q.R., Wang, F.Y., Lin, C.J., Zhang, L.M., Hui, M.L., Hao, J.M., 2016. Mercury transformation and speciation in flue gases from anthropogenic emission sources: a critical review. Atmos. Chem. Phys. 16, 32889–32929.
Zheng, W., Foucher, D., Hintelmann, H., 2007. Mercury isotope fractionation during volatilization of Hg(0) from solution into the gas phase. J. Anal. At. Spectrom. 22, 1097–1104.
Zhou, Z.J., Liu, X.W., Zhao, B., Chen, Z.G., Shao, H.Z., Wang, L.L., Xu, M.H., 2015. Effects of existing energy saving and air pollution control devices on mercury removal in coal-fired power plants. Fuel Process. Technol. 131, 99–108.